Journal of Power Sources 195 (2010) 8124–8133

Contents lists available at ScienceDirect

Journal of Power Sources

journal homepage: www.elsevier.com/locate/jpowsour

Acoustic emission: Towards a real-time diagnosis technique for Proton Exchange Membrane Fuel Cell operation

B. Legros[a,b], P.-X. Thivel[a], Y. Bultel[a], M. Boinet[c], R.P. Nogueira[a,*]

[a] LEPMI, UMR 5631 Grenoble INP-CNRS-UJF, 1130 rue de la piscine, BP75, 38402 Saint-Martin-d'Heres Cedex, France
[b] SIMAP, UMR 5266 Grenoble INP-CNRS-UJF, 1130 rue de la piscine, BP75, 38402 Saint-Martin-d'Heres Cedex, France
[c] Euro Physical Acoustics SA, 27 rue Magellan, 94373 Sucy en Brie, France

ARTICLE INFO

Article history:
Received 14 April 2010
Received in revised form 7 June 2010
Accepted 17 July 2010
Available online 22 July 2010

Keywords:
Fuel cell
Monitoring
Non-destructive testing
Water management

ABSTRACT

This paper deals with one of the needs for PEMFC to be economically reliable: diagnosis tool for water management. This issue is actually a key parameter for both performance and durability improvement. Acoustic emission (AE) technique was employed to survey PEM single cell under various operating conditions. AE events coming from different sources have thus been identified, classified and finally ascribed to different phenomena induced by MEA water uptake and/or biphasic flow in the gas channel thanks to a statistical post-treatment of the acoustic data. Results, although qualitative, seems trusty enough to unravel hidden correlations between AE hits and physicochemical phenomena taking place during the cell operation and open up the way for an innovative and non-invasive online diagnosis tool.

1. Introduction

The Proton Exchange Membrane Fuel Cell (PEMFC) seems to be a promising energy converter for various power applications. Nevertheless, in spite of undeniable progresses undergone both in scientific knowledge and technological development, PEMFC assemblies and parts still present certain drawbacks and improvements must be made such that the system is reliable for industrial applications [1–5]. Cost reduction, reliability and performances thus remain strong research issues [6–8] as well as cell diagnosis [9–12].

Among the numerous phenomena that occur during cell operation, water behavior is still not completely understood and remains difficult to survey. This is a major issue as water management is well-known to be tightly related to both PEMFC reliability and performances [5,10–12]. Improving or optimizing water management during the cell operation is thus a subject of crucial point which is object of continuous and diversified research effort [13–18].

Water management must take into account processes occurring in gas channels, across the gas diffusion layers (GDL) and inside the Nafion membrane. This simultaneity makes the overall problem quite complex and difficult to handle. This can be illustrated by the fact that whereas Nafion needs to be highly hydrated for best performances, GDL and gas channel must be protected from flooding. Some of the main parameters and phenomena that have to be managed are hence relative humidity (RH) and water droplet formation in gas channel as well as the water level in both the GDL and the Nafion membrane. Water is produced through the electrochemical reaction and the reactant gas can be humidified to help the humidification of the membrane and so to increase its ionic conductivity. On the other hand, water transport in the membrane is leaded by electro-osmotic drag and back-diffusion. The ideal water level is therefore not easy to determine experimentally and difficult to maintain especially without trustworthy in situ water level measurements.

Usual experimental methods based on different techniques devoted to the evaluation of cell state (electrochemical impedance spectroscopy [19], current interruption [20], pressure drop [21,22], and so on) are certainly powerful but remain not suitable to deal with the transient, heterogeneous and even stochastic aspects of the phenomena taking place in the MEA. Indeed, owing to the cell geometry, the uniformity of the chemical, physical, and electrical values is never perfectly achieved. In this sense, a technique allowing measurement of membrane hydration state and which should be sensitive to localized phenomena would be of major interest towards the development of better water management strategies. Using neutron radiography with a miniaturized PEMFC under operative condition, Seyfang et al. [23] visualized the liquid water and the water profile from cathode channel to anode channel showing the accumulation of water in the cathode catalyst layer. Such acquirements are to date only provided by neutron imaging [5–23] which needs rare and expensive facilities.

* Corresponding author. Tel.: +33 4 76 82 65 93; fax: +33 4 76 82 67 77.
E-mail address: ricardo.nogueira@grenoble-inp.fr (R.P. Nogueira).

0378-7753/$ – see front matter © 2010 Elsevier B.V. All rights reserved.
doi:10.1016/j.jpowsour.2010.07.045

In the field of instrumentation and monitoring techniques, non-destructive testing has a large range of applications thanks to numerous non-invasive techniques. Among them acoustic emission (AE) seems to have a strong potential for PEMFC water management investigation. AE technique is based upon the fact that, when undergoing mechanical solicitation—even at a local level, materials can spontaneously generate transient elastic waves, called acoustic emission. Each AE event gives rise to elastic waves which propagate into the material yielding detectable AE signals allowing the detection of active defaults within materials on a real-time and continuous basis during the test and being hence prone to be used in the industry either for process monitoring, material characterization or damage assessment [24]. The variety of mechanism of deformation and damage that can be sources of AE are numerous [25]. Among them, AE has already been used to study or monitor electrochemical phenomena as anodization [26], corrosion [27,28] or even oxygen reduction [29].

To our knowledge, although some attempts have been successfully done to fuel cell thermo-mechanical behavior monitoring in the case of solid oxide fuel cells [30], AE has not been used or evaluated for PEMFCs application. It has however been shown that Nafion structure depends on its water content [31,32] and thus that its evolution gives rise to considerable structural changes. The cyclic stress and dimensional change induced by the water uptake can be substantial and are the main causes for the mechanical degradation of the membrane [33] that can be supposed to trigger AE events. In a previous work [34], AE activity recorded on Nafion membrane under dehydration in a climatic chamber has been investigated. It has been demonstrated that dehydration process trigger AE events that can be sensed by an appropriate sensor. Furthermore, AE technique has shown an ability to detect dehydration phenomena at its last stages, which are not sensed by electrochemical impedance spectroscopy. These results open up the way to deeper investigations of structural changes that take place during membrane dehydration and also to the development of real-time PEMFC diagnosis devices.

The present paper goes deeper in this later direction. As AE technique has shown an ability to detect dehydration phenomena [34], AE events can also result from liquid water removal from the inner part of the cell, the catalyst layer, to the gas channel. This work tries to identify and classify AE events according to their physical source so as to ascribe typical signal fingertips to some cell operation parameters or behaviors. This was achieved with the help of specific experiments under controlled conditions to maximize or on the contrary minimize (or even preclude) different AE potential sources. As will be discussed in what follows, some fingertips were more or less easily undisclosed but it seems that, due to the complex and simultaneous nature of the undergoing phenomena during PEMFC operation, most of the information is hidden within an entangled joint evolution that needed a statistical post-treatment.

2. Experimental

2.1. Measuring devices

In situ study on operating PEMFC was carried out using a single cell with a 25 cm^2 Paxitech® Membrane Electrode Assembly (MEA). The MEA was made of Nafion membrane (thickness 50 μm) and a gas diffusion electrode. The platinum loads of the Paxitech electrode were 0.6 mg cm^{-2} for both anode and cathode and the gas channels had a square section of 1 mm^2 engraved into graphite plates. The cell was fed with pure hydrogen and oxygen or a mixture of nitrogen and oxygen in the cathode side. The fuel cell operated thanks to a test bench that independently controlled fluidic (flow rate, pressure, gas humidification, gas temperature and gas composition) and electric circuits. Before each experiment, a 1 h long wait time in operating conditions was applied to reach steady and reproducible starting conditions.

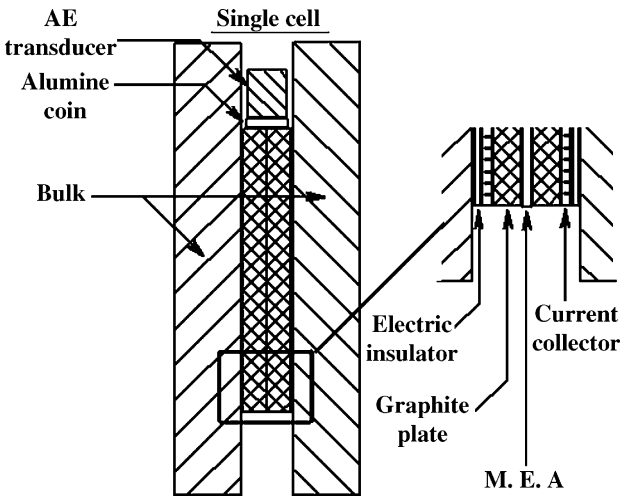

Fig. 1. Experimental set-up for in situ AE signal acquisition.

AE signals were acquired thanks to the experimental set-up depicted in Fig. 1. A piezoelectric sensor (resonant frequency of 175 kHz and frequency range of 50–200 kHz) was placed above the graphite plates and coupled with silicon grease—a small alumina coin was inserted between the graphite plates and the sensor to protect the cell from short circuit. The dimensions of the piezoelectric sensor were 16 mm in diameter and 16 mm height. In cases where not enough place is available to directly pin the sensor against the cell, a wave guide can be used to convey the signal to the sensor. The sensor converts the mechanical waves into electrical signals related to AE events which appear in the form of bursts or hits that can be surveyed against time. AE signals were filtered (20–1200 kHz) and amplified (40 dB gain), and processed by the acquisition system. The coupling check of sensor is performed before and after each test with the Hsu-Nielsen calibration source [35].

The sensitivity of an acoustic emission system is often limited by the amount of background noise nearby. Noise in AE testing refers to any undesirable signals detected by the sensors. To compensate for the effects of background noise, various procedures can be implemented. Some possible approaches involve the use of special sensors with electronic gates for noise blocking, choosing convenient locations to place sensors as far away as possible from noise sources, and electronic filtering. Furthermore, prior to any AE experiment, a recording threshold value must be defined. This threshold is the limit beyond which the acquisition system will take the corresponding burst into account and record it allowing further data treatment to be done later. A threshold value of 30 dB_{AE} was chosen, which, after blank experiments, appeared to be an appropriate value to study PEMFC in the experimental conditions held for the present study and prevent from recording acoustic emission signals drowned by background noise.

2.2. AE data treatment and analysis

The discrimination between the different sources of AE signals can be a difficult task when the signal coming from each individual source may overlap with others originating at different locations and phenomena, which is certainly the case of PEMFC operation due to the simultaneous occurrence of multiphase transport, such as gas phase and liquid water in the different sub-domains of the cell. In such cases, automated statistical and/or neural network techniques

can extend the AE user's capabilities in identifying the hidden structure and correlation of data categories in a multidimensional space. It is important here to stress that, although this is a major issue for the analysis and discussion of the experimental data presented in the next sections, it is far beyond the aims of the present paper to go deep in the huge concern of statistical post-treatment. The interested reader is invited to refer to the vast literature devoted to this subject (see for instance Refs. [36,37] for Principal Component Analysis and pattern recognition, respectively). We tried to give here only the minimal information deemed necessary to the self-readability of the paper.

In this study, statistical post-treatment based upon Noesis® facilities was employed to gather qualitative information on the origin of the AE events measured during PEMFC operation in different conditions. More precisely, Principal Component Analysis (PCA) first allowed the discrimination between data coming from distinct origins and hence their classification into different clusters or classes. Afterwards, a supervised pattern recognition (SPR) algorithm was employed to train the software to recognize signals belonging to those previously established classes of AE events.

The PCA started by assimilating each AE hit to a vector, the coordinates of which correspond to the various AE parameters. Each vector is represented in a multidimensional space baring as many dimensions as the number of considered AE parameters. Separating the experimental vectors into well identified populations of events includes several steps. The first step was to select a representative set of AE features based on which data exhibiting similar characteristics would be segregated into classes. For that purpose, feature correlation analysis was performed for all the AE features held. Then, all features were normalized individually to a range from −1 to 1, in order to avoid biasing the classification towards the feature exhibiting the highest physical dimensions. In fact, similarity cannot be properly detected when different units of measurement, value range, etc. might bias the data. Moreover, instead of working with this complex multidimensional space, it is possible to work with for instance two-dimensional projections in axis spaces chosen according to the level of information they convey, which is related to the eigenvectors and eigenvalues of the correlation matrix of the normalized parameters.

In the present study, the clustering was performed manually, i.e. by ranking data according to the type of experiment performed. The operating conditions were indeed chosen to obtain specific events and avoid as long as possible the concomitant occurrence of other undesirable superimposing events, as explained in Section 3.

Once clusters or classes of signals have been created, SPR was performed for the classification of new AE data. To do this, SPR algorithms first need to be trained to recognize the original classes and, once the training is completed within satisfactory error margins, be applied to classify new data. This is achieved by feeding the SPR algorithm with a set of training data of well-known characteristics that constitutes a typical fingertip of a certain behavior or, in other words, belongs to a class or cluster. After this learning step, once confronted to new unknown experimental data sets, the algorithm searches for hidden similarities with the previous training data set that, whenever present, are identified and labeled as belonging to that cluster. More precisely, the SPR algorithm assimilates to the trained cluster not only those hits having exactly the same characteristics, but also those inside a close vicinity of the original parameters values. The spread of this neighbourhood is defined by the user and constitutes one of the main over or underestimation error sources of the SPR procedure. This is why once trained, the SPR procedure must be verified with the help of a testing data set, also of well-known characteristics but distinct from and obviously not employed as the training data or part of it.

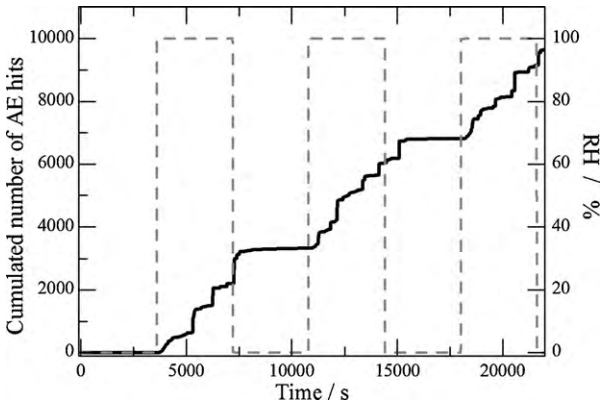

Fig. 2. Time evolution of the cumulated number of AE hits (black solid line) and the square-shaped switch on–off of the relative humidity of feeding gases (gray dashed line); gas flow 1.4 L min^{-1}: O_2 = 0.2 L min^{-1}; N_2 = 0.8 L min^{-1}; H_2 = 0.4 L min^{-1} at 60 °C.

3. Results and discussion

The appropriate analysis of AE signals coming from multi-source complex events as those generated by an operating PEMFC underscores the need of a previous identification and classification of typical fingertips or characteristic parameters related to these different sources. Hydrodynamic conditions in the gas channel, liquid water transport within the GDL and the gas channel, as well as membrane drying or dehydration are all potential sources of acoustic activity one has to separately handle to be able to analyze raw signals coming from real operating cells. In this sense, we have performed different categories of experiments to try to check out their AE activity and, if possible, identify the signal profiles or characteristics that could be unambiguously linked to different phenomena. These controlled experiments were also conceived to allow different classes to be built up as described later.

3.1. AE activity due to hydrodynamic effects into the gas channels (cell with a silicon seal in place of the MEA)

A first set of experiments was hence performed so as to isolate pure hydrodynamic phenomena from the gas channel. In this sense, experiments were carried out without MEA (hereafter referred to as NO_MEA), which was replaced by a silicon seal separating the anodic and cathodic sides. The aim of this experimental step was to study the acoustic emission coming from the gas flow in the fuel cell channels without any indirect electrochemical considerations. Two main hydrodynamic events are expected to be at the origin of acoustic emission: on one hand, hydrodynamic effects in the flow in particular at high flow rate and on the other hand, the presence of water droplets circulating in the gas channels. Evidently, under common PEMFC operating conditions, there exist a substantial amount of liquid water inside the cathode flowfield as well as on the GDL surface. At the interface of GDL/channel, water droplets build up and, after an irregular delay, the droplets aggregate and block the gas channels and/or water is removed through the gas channel either in liquid form or in vapour phase. Liquid droplets in the gas channel are observed due to liquid water interactions with the channel walls and water drainage from the channel.

The influence of water in gas channel was investigated by intermittently switching the gas flow from humidified to non-humidified conditions at a fixed flow rate. Fig. 2 shows the time evolution of the cumulated number of acoustic events in parallel to the square-shaped humidification management of the feeding gas at 60 °C and a cell temperature maintained at room temperature so as to favor condensation. It clearly appears that no AE activ-

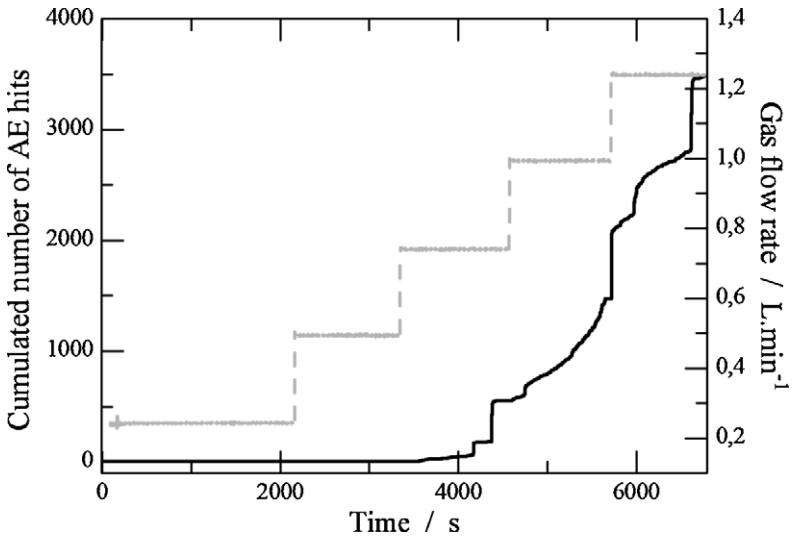

Fig. 3. Time evolution of the cumulated number of AE hits (black solid line) and the controlled profile of the steeped increase of feeding cathodic gases flow rate at 60 °C (gray dashed line).

ity is sensed during the dry cycles. On the contrary, humidification always entailed a significant activity in the form of bursts which are to be associated to biphasic flow, water droplet circulation or other hydrodynamic phenomena. A sharper analysis of Fig. 2 indicates a certain delay of AE activity to vanish after the humidification is shot off probably due to residual humidity at the gas channel and/or the system operation inertia.

It is worth noticing that Fig. 2 has been obtained in harsh conditions due to a fixed high level gas flow, 1.0 L min^{-1} in air and 0.4 L min^{-1} in H_2, not representative of usual operation conditions of PEMFC, as discussed later. The effect of the flow rate in the AE activity was hence investigated by proceeding to a stepwise modulation of the flow rate of permanently humidified gas as shown in Fig. 3. Both anodic and cathodic gas flow were increased step by step to reach respectively the value of 0.4 and 1.25 L min^{-1}. As the higher flow rate is the most representative, only cathodic gas flow is represented in the figure. For gas flow lower than 0.75 L min^{-1} (which corresponds to a Reynolds number of 830), a flat AE signal clearly indicates that no specific AE events occurred. Beyond this threshold value, AE activity drastically increased notwithstanding the fact that, whatever the flow in Fig. 3, the hydrodynamic regime remained laminar (Re < 2000 [18]). In spite of this macroscopic laminar behavior, the existence of local (space and time) turbulences cannot be disregarded—especially at channels edges. The increase of AE activity is thus probably due to biphasic flow effects, for instance, those drag effects related to water droplets of increasing velocity sliding along the gas channels walls. Even if high AE activity is observed for higher flow rate, not representative of usual operation condition of PEMFC, the water quantity in the gas channel is also lower in our operation condition (NO_MEA). Largest water quantities will be observed in the case of an operative PEMFC owing to the water production by the electrochemical reaction at the cathode side.

These first experiments investigate the influence of hydrodynamic in the gas channel. At this step, two important points deserve specific comments. First, the gas composition has been investigated and shown no influence in terms of AE activity. Pure hydrogen, pure nitrogen, pure oxygen and a mixture of nitrogen and oxygen were tested with no significant changes in the results or in the threshold value for AE detection. It can be stated that monophasic gas flow is not at the origin of AE activity. Secondly and more important, an AE activity was recorded until a fully humidified gas at flow rate larger than 0.75 L min^{-1} fed the cathode. This 0.75 L min^{-1}-threshold is largely beyond the gas flow rate effectively needed to optimal operation conditions in our experimental set-up. Indeed, for a current density of 1 A cm^{-2} and a 1.5 overstoechiometric factor, the flow rate is 0.14 L min^{-1} in cathodic side and 0.28 L min^{-1} for anodic side. Nevertheless, this means that the existence of AE activity can be ascribed to diphasic flow in the gas channel. It is worth mentioning that water production strongly increases when a current is flowing the cell, increasing probably AE activity.

3.2. AE activity in the presence of MEA

In the present section we come back to the conventional set-up by introducing the MEA in the place of the silicon seal. This brings to the forefront of the problem of identifying possible AE sources the effects of the interactions of humidified gases with GDL porous media and possible indirect effects induced by electrochemical reactions. The measurements were hence split in two main experiments: at open circuit (no electrochemical reaction effects expected), and under normal operation conditions, that means, current delivering cell.

The first measurement was carried out in the same conditions as those of Fig. 2, that means, intermittently humidified non-humidified high rate gas flow: 1.0 L min^{-1} in air and 0.4 min^{-1} in H_2), but in the presence of MEA at open circuit potential. As it can be seen in Fig. 4, the AE behavior is qualitatively similar to the previous experiment without MEA, that is, no AE activity during dry cycles and a bursted increase otherwise. The AE activity in Fig. 4 is represented in terms of cumulated absolute energy of the hits to illustrate the fact that AE technique can yield different significant parameters (the plot of cumulated number of hits as in Fig. 2 also gives the same qualitative results).

Taking advantage of this multi-criteria feature of AE technique, a first attempt to identify the characteristic profile of AE signals in the absence (NO_MEA) or in the presence of MEA at open circuit potential (MEA_OC) was performed by straightforwardly comparing some typical AE parameters issued from the signals at each condition, as illustrated in Table 1. It appears that the presence of MEA constitutes a kind of brake on each elementary event. Indeed, hits are slower (higher mean duration), less energetic (mean absolute energy) and more inertial (higher mean rise time). This can probably be ascribed to two specific AE activities depending on the assembly investigated. In the absence of MEA, the humidified gas flow inside the gas channels easily slides along the smooth,

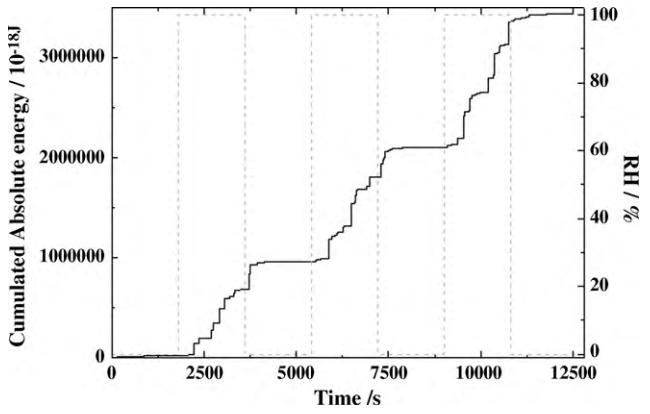

Fig. 4. Time evolution of the cumulated absolute energy of AE hits (black solid line) and the square-shaped switch on–off of the relative humidity of feeding gases (gray dashed line); gas flow 1.4 L min^{-1} (O_2 = 0.2 L min^{-1}; N_2 = 0.8 L min^{-1}; H_2 = 0.4 L min^{-1}) at 60 °C.

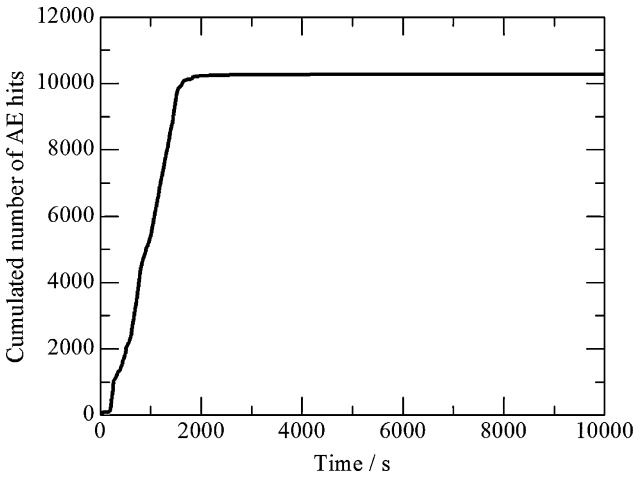

Fig. 5. Cumulated number of AE hits during the full dehydration of a MEA purged with dry reactant gas at 60 °C (O_2 = 0.2 L min^{-1}; N_2 = 0.8 L min^{-1} and 0.4 L min^{-1} hydrogen) after a 80 h hydration procedure by completely filling the gas channels with deionised water.

impermeable and inert silicon seal. In the other case, due to interactions with MEA, the signal is characterized by slowing down effects (hence slower and less energetic AE events) related to the fact that the diphasic flow now rubs against a rougher surface, goes through a porous media and is indirectly controlled by the humidification of the GDL and the membrane.

The hypothesis that water removal from MEA could be a potential source of AE activity was verified by performing a dehydration experiment. This hypothesis is supported by results from a previous work [34] in which AE was shown to be sensitive enough to detect structural changes taking place during membrane dehydration. Due to water production, liquid water fills the porosity of both active layer and gas diffusion layer. Moreover, liquid water transport in the GDL is essentially a drainage process governed by capillary and viscous forces into the complex pore network and those phenomena are expected to trigger AE events. MEA was hence first fully hydrated by completely filling the gas channel with deionised water. After 80 h cell was purged with dry reactant gas at 60 °C (1 L min^{-1} air and 0.4 L min^{-1} hydrogen) and the AE activity was recorded during the drying of the MEA (Fig. 5). The total time for a complete water removal and membrane dehydration in these conditions is about 1500 s (corresponding to the onset of AE activity plateau) which can explain the delay observed during the cycling runs in Figs. 2 and 4. The EA activity can be ascribed to water removal from the complex network of gas pore of the GDL to form water droplet and the subsequent water droplet circulation along the gas channel.

Finally, to investigate the AE activity of a running PEMFC, new experiments were performed in which the cell was subjected to current steps (MEA_CS) to evaluate AE activity incorporating effects indirectly related to electrochemical reactions. The idea behind this procedure was that water production by the oxygen reduction at the cathode can exacerbate the AE activity. In that case, the increase of the liquid water flow through the complex network of the MEA and gas channel should result in AE activity intensification. These measurements were carried out so as to avoid any AE phenomena linked to hydrodynamic in the gas channel. The cell was hence operated at 60 °C with non-humidified gas, pure oxygen and hydrogen at constant flow rate below the critical one determined previously (0.35 L min^{-1} for both sides which corresponds to an overstoechiometry factor of 4 and 2 for O_2 and H_2, respectively). The current steps consisted of 30 min Open Circuit Voltage (OCV) followed by 30 min at 1 A cm^{-2} (25 A). The cumulated AE activity and the current value are plotted in function of the time in Fig. 6. Even if lower anodic and cathodic flow rates are considered (<0.75 L min^{-1}), AE activity is observed. This intensification at low flow rate can be related to the largest water production when cell is running. Unlikely to previous experiments NO_MEA and MEA_OC, where AE activity only occurred when triggered by the square-shaped humidity level (cf Figs. 2 and 4), the signal is now much less synchronous regarding the current steps. This means that AE occurred not only when the cell was under solicitation, but also during the switched-off periods, notwithstanding the fact that AE activity response was clearly causal, that means, it was triggered by the first current solicitation step. Qualitatively, the AE signal shows shorter periods of intensified activity and larger inhibited ones. Even if one can intuitively try to correlate boosted (conversely inhibited) activity to current solicitation (conversely interruption), the shift between these two regimes is not straightforwardly triggered by switching on/off the current solicitation. It is worth noticing that this experiment has been performed several times, always delivering this non-correlated evolution from

Table 1
Mean value of typical AE hits parameters for NO_MEA and MEA_CS experiments.

	Mean duration (μs)	Mean rise time (μs)	Mean absolute energy (aJ)
NO_MEA	385	125	151
MEA_OC	509	209	99

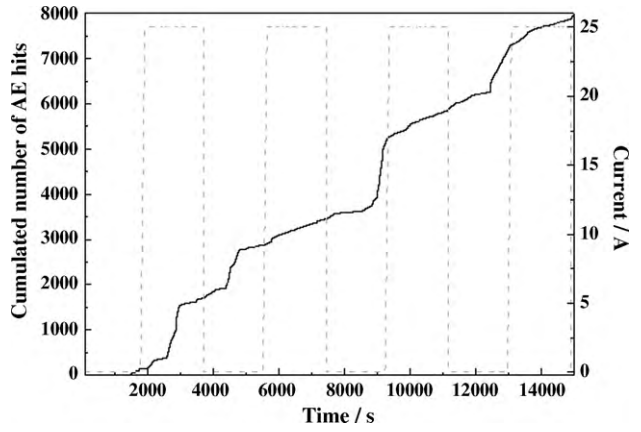

Fig. 6. Time evolution of the cumulated number of AE hits (black solid line) and the square-shaped switch on–off of the 1 A cm^{-2} (25 A) current solicitation; gas flow 0.7 L min^{-1} (O_2 = 0.35 L min^{-1}; H_2 = 0.35 L min^{-1}) at 60 °C.

which Fig. 6 is a typical illustration. It hence seems that the overall behavior of AE activity under intermittent current solicitation convey combined effects from complex and simultaneous events taking place at different levels of the MEA. From this point of view, acoustic behavior can be directly related to water production by electrochemical reaction such as: water uptake or desorption in the membrane, filling AL and GDL porosity, water transport through the GDL, water droplets build up at the GDL/channel interface and diphasic flow in the gas channel. These phenomena are complex and irregular, which can explain the non-predictable time delays between the instant the current is switched on (off) and the intensification (inhibition) of the AE activity starts. This result agrees with the total time of about 1500 s for a complete water removal and membrane dehydration.

Since Figs. 2 and 4 have shown that purely hydrodynamic effects in the gas channel or simple non-reactive MEA interactions evolve rather synchronously with the cell perturbation, it is reasonable to ascribe the complex and randomly distributed behavior depicted in Fig. 6 to the parallel occurrence of water production by the electrochemical reactions. Indeed, capacitive behaviors, or large time constants phenomena can delay the system response and made it non-synchronous regarding the interface perturbation represented by the squared current solicitation profile. Electrochemical effects on the AE activity are indirect in the sense that they are related to local mechanical stresses relaxation induced by water removal from inside the catalyst layer to the gas channel through the gas pore network of the GDL or structural changes taking place during the membrane hydration.

This first part of the study clearly indicates that AE technique is sensitive to phenomena taking place during PEMFC operation, which confirms results from some few previous studies [30,34]. Whatever the exact causes of the complex evolution depicted in Fig. 6, however, this non-synchronous behavior makes any simple and unambiguous monitoring strategy difficult to be implemented for the real-time survey of an operating PEMFC. Furthermore, the simplified procedure of just counting AE events in these complex conditions does not convey enough information about the sources underneath these events. In the next section a less simple but more powerful post-treatment analysis strategy based on statistic tools is proposed to deal with those complex results.

4. Post-treatment and statistical analysis

As presented in Section 2.2, it is possible to proceed to a sharper and deeper analysis of the AE results by a suitable post-treatment and statistical analysis. Let us start by proposing an ansatz which consists in considering that the AE data that have been recorded during NO_MEA, MEA_OC and MEA_CS experiments presented above can be separated according to their source and classified into 3 classes:

- *Class A*: Phenomena that take place in the gas channel, i.e. those related to diphasic flow or water droplet circulation in our hydrodynamic conditions (hydrodynamic effects).
- *Class B*: Phenomena that take place in both the GDL and the gas channel, i.e. those related to water removal from the GDL to the gas channel (so-called non-reactive interactions between gas and MEA).
- *Class C*: Phenomena related to water uptake and desorption in the catalyst layer (filling of the porosity of the active layer (AL)) and membrane (swelling, shrinking) That include membrane shrinking and swelling due to water level decrease and increase, and water transport into the membrane and the catalyst layer (so-called reactive interactions).

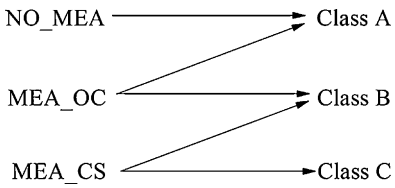

Fig. 7. Synoptic description of the classification of AE events coming from different experiments.

The idea behind this classification is hence to establish a relationship between these classes of hits and the AE sources. This should allow any experimental data to be split into different classes and hence be understood in terms of which elementary physical events were taking place during the cell operation under well-defined experimental conditions and this should be the early basis of an effective monitoring strategy.

To build each one of these classes, it is worth noticing that if some data can be easily ascribed to one of these classes thanks to the experimental procedure, most of it needs further processing as statistical discrimination as described in what follows with the help of the synoptic classification depicted in Fig. 7. The whole data set of the NO_MEA experiment can be ranked in class A but this is the only straightforward classification allowed, the other experiments being composed of more than one single source of AE events. Indeed, data coming from the MEA_OC experiment, which contains both hydrodynamic and MEA interactions, must be separated within classes A and B (but not class C due to the absence of electrochemical reactions). This means that NO_MEA experiment feeds class A only, but class A contains data from both NO_MEA and MEA_OC.

Class B is thus to be filled by MEA_OC experiment (excepted from the purely hydrodynamics events attributed to class A) but also by the "non-reactive" part of MEA_CS events, whilst class C is supposed to be filled only by the "reactive" part of MEA_CS events. It holds that class C is the only to be fed by only one experiment. Therefore, the first step is to identify the data (parameters and range of values) that are exclusively characteristic of MEA_CS (the "reactive" part of it, that is, events related to electrochemical reactions) and hence build class C.

Before going further in this classification we should first identify, among the several features of AE events, which parameters convey discriminating information. We start by choosing five AE parameters having an universal character, that means, easily and intuitively identified in any AE burst: rise time, counts till peak, total counts, duration and peak amplitude as schematically represented in Fig. 8. This choice means that the experimental raw data set could be now

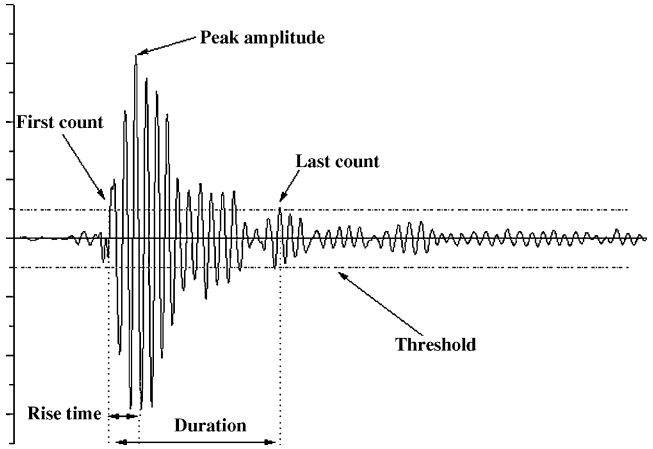

Fig. 8. Schematic representation of a single burst (a hit) and some of the characteristic features held for the statistical post-treatment.

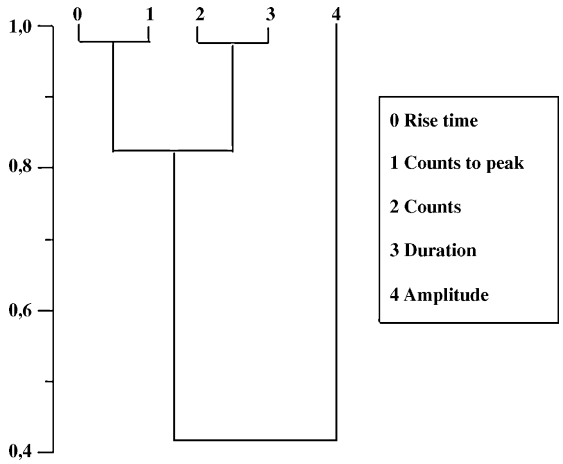

Fig. 9. Dendrogram of the hierarchic correlation between the characteristic parameters of AE hits held for the statistical post-treatment.

represented by a five-dimension points cloud referred to a 5-axis system—one for each parameter held—not mutually independent. Fig. 9 shows their unsupervised classification in the form of correlation hierarchy as a dendrogram obtained from the ensemble of the data coming from experiences NO_MEA, MEA_OC and MEA_CS. An intuitively expected close correlation appears, for example, in the case of numbers of counts and burst duration (>0.95) whilst a much weaker correlation stands for the amplitude and the other four parameters (≅0.4).

Considering that different AE sources can yield bursts with different characteristics, the direct comparison between these high correlated parameters for each kind of experiment would, at least a priori, be an interesting possibility to discriminate different experimental conditions and thus allow the implementation of the different classes. Fig. 10A–D illustrates this issue with the help of the raw number of total counts and the duration of each burst for the three experiments, that means, the projection of the five-dimension raw data points cloud in the two-dimension counts vs. duration space plotted in the same scale to allow direct comparison between the different conditions. As expected due to the high correlation level, points tend to merge according to a linear behavior in which one can see that experiments NO_MEA and MEA_OC spread all long the overall range (Fig. 10A and B, respectively) whilst MEA_CS is confined to the low range values (Fig. 10C). This means that high values of count numbers and duration are most related to a high hydrodynamic activity characteristic of the NO_MEA and MEA_OC cases, that could thus be isolated and associated to big bursts. On the other hand, MEA_CS experiments cannot be discriminated from this analysis since its characteristic space superimposes to the other experiments, also represented in the low values region (Fig. 10D). Collecting data in the range [0,500] for the counts and [0,5000] for the duration would encompass events coming from all the experiments, which means that this projection based on the raw data values has no discriminating power and does not allow class C to be implemented (as explained before, class C should be the first to be built since the only one to be fed by a single experiment as depicted in Fig. 7).

We hence proceeded to a Principal Component Analysis, in which each parameter, instead of bringing its raw values as in Fig. 10, is normalized between −1 and 1. The new points cloud is associated to a set of five new axis (the same number of burst parameters retained in the dendrogram of Fig. 9), built up from the diagonalization of the correlation matrix and labeled as axis 0–4 from the higher to lower eigenvalues (the higher the eigenvalue associated to an axis, the higher the information level this axis conveys). This means that the two principal axis (0 and 1) are

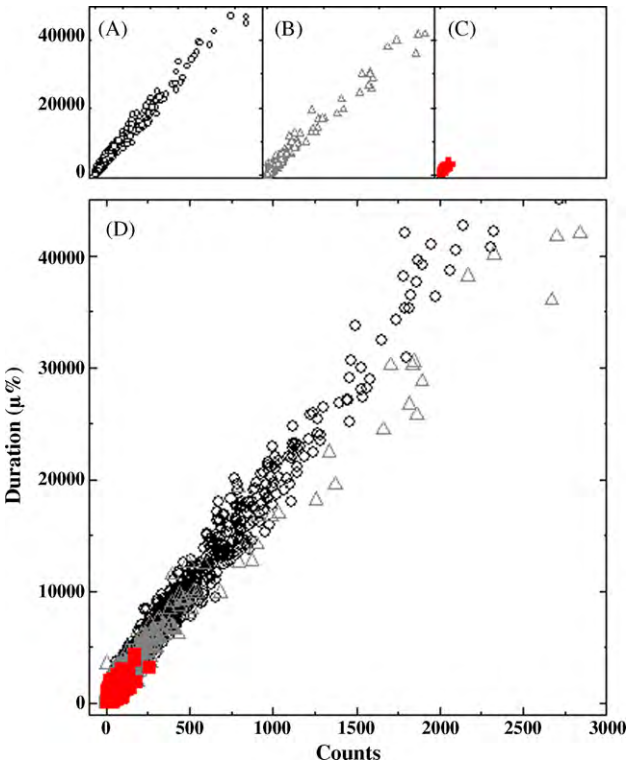

Fig. 10. Raw data projection in the number of total counts vs. duration space for each individual experiment NO_MEA (A, ○), MEA_OC (B, △) and MEA_CS (C, ■) and the merged behavior (D). All windows depicted in the same scale.

those that better represent the new points cloud. We can now proceed to the same kind of projection as in Fig. 10, notwithstanding the fact that, due to the mathematical treatment, the new axis has no clear physical meaning. What is interesting in this procedure is that one can be sure that this projection will reflect, in the new PCA 0–1 axis space, the higher level of information one could get from the original data set. Fig. 11 shows the result of the PCA 0–1 axis projection of the ensemble of points from the three experiments. Unlikely to the direct projection in Fig. 10, a non-negligible part of experiment MEA_CS is now clearly isolated in the right side of the PCA 0–1 space as indicated in the figure. Effectively, events represented in the surrounded part of Fig. 11 correspond to 8% of the data coming from MEA_CS and less than 0.2% for the other experiments.

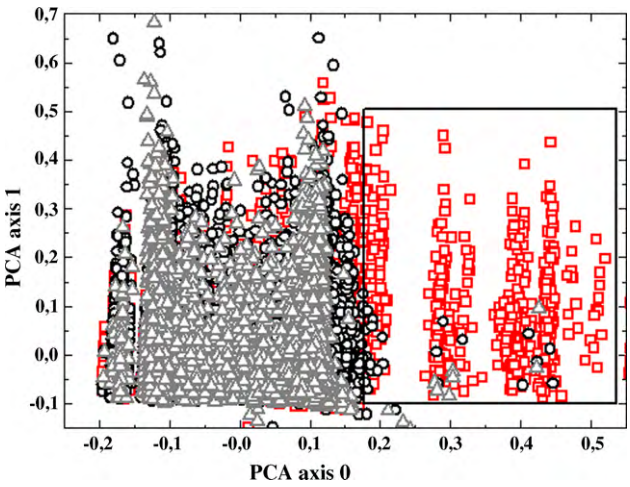

Fig. 11. PCA projection in the 0–1 axis space for each individual experiment NO_MEA (○), MEA_OC (△) and MEA_CS (□).

This region of the PCA 0–1 axis space can thus be unambiguously ascribed to electrochemical-based events susceptible to take place during the MEA_CS experiment but not during the others and were used to build up class C, that means, the one related to electrochemical reaction effects and the only one to be fed by a single experiment as mentioned before.

Following the schematic description of Fig. 7, once class C was created, part of class B could be built up with those events coming from MEA_CS and not previously allocated to class C, which are supposed to correspond to MEA interaction with weak hydrodynamic flows. Class B should however also encompass some of the events coming from MEA_OC related to the interaction between MEA and strong hydrodynamic activities (the remaining data from MEA_OC going to class A, purely hydrodynamic effects). To split MEA_OC into classes A and B events, supervised pattern recognition method was employed. The training data set was composed of both NO_MEA and MEA_CS, the latter being nevertheless naturally expurgated of events previously ranked into class C.

In a first step, SPR collected and analyzed data coming from these two categories so as to further recognize events related to purely intense hydrodynamic data in the absence of MEA (NO-MEA) and data from the interaction between MEA and weak hydrodynamic flow without current (assimilated to those coming from the MEA_CS expurgated of class C data). Once trained, the method was applied to MEA_OC signals. What has not been recognized as one of this two attributes (high hydrodynamic activity or MEA and weak hydrodynamic interactions) were considered as being the interaction of intense hydrodynamic flow and the MEA and allocated to complete class B.

Finally, class A was fed by the totality of events from NO_MEA plus those coming from MEA_OC events not ranked into class B.

The three classes being created, the overall post-treatment procedure could thus be trained and improved by performing post-analysis of signals of the same type of those previously used to built up the classes. The training data were therefore sets from equivalent experiments performed in the same experimental conditions. As an example, a new MEA_OC experiment performed in the same experimental conditions (temperature, fluidic) was expected to bring again a AE hit distribution to be split between classes B and C.

After this consolidation stage, the pattern recognition method was ready to be applied to new experimental data that could be normalized, retreated with the same five parameters depicted in the dendrogram of Fig. 8, projected in the new PCA 0–1 axis space and confronted to the classes distribution. The method is then likely to determine from any new experimental data how much of it corresponds to each class, and hence survey the presence of strong or weak hydrodynamic evolution, non-reactive MEA interactions or indirect electrochemical reactions effects.

The goodness of the method should be finally evaluated with different experiments from which one could reasonably anticipate the AE sources involved so as to validate the results obtained.

This was first achieved with the help of the experiment illustrated in Fig. 4 (MEA dehydration), since it was not used to build up the classes. It hence constituted the testing data set for the supervised pattern recognition method. Because this experiment was conceived as a high rate dehydration one (the membrane was fully flooded and dried by forced convection in contact with high flow rate dry gases, hence not conveying any electrochemical reaction), one should expect a weighed A > B > C classes distribution. The results obtained were identified as 63.5% coming from class A, 33.1% from class B and 3.4% from class C, which is in good agreement with the experiment nature.

In the case this primary classification is not exhaustive, that means, results remain not clearly discernable by the pattern recognition methods, the procedure can be extended to other PCA axis

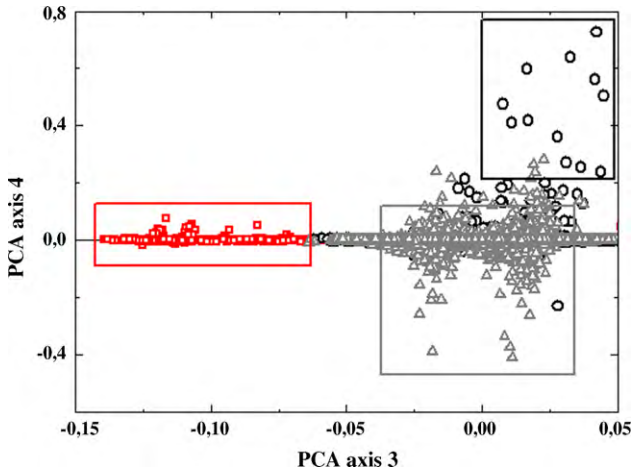

Fig. 12. PCA projection in the 3–4 axis space for each individual experiment NO_MEA (○), MEA_OC (△) and MEA_CS (□).

spaces, or in other words to other projections of the points cloud. Fig. 12 illustrates this issue with the PCA 3 vs. 4 axis space. It can be seen that this plan also gives an interesting alternative to at least partially separate experiments, in spite of a strong collapse of points along the PCA axis 4 origin. Experiments seem to be clearly discernable inside discriminating sectors as indicated in the figure. Although conveying less information, these secondary axes can complement or constitute a second level of analysis to validate results coming from the primary classification or to settle about inconclusive data.

The second experiment used to validate our study concerns a fuel cell undergoing a phenomenon of flooding. Fig. 13 shows the evolution of the voltage and current density vs. time. After a 30 min OCV period, a current ramp of 0–15 A was applied. A difference of 10 °C is maintained between gas and fuel cell to promote water condensation. From about 4000 s, a voltage drop related to cell flooding clearly appears. The AE activity (Fig. 14) is present during the whole experiment due to humidified gas flow at high temperature. It should be noticed that the first 1000 s are not performed at stabilized gas temperatures and humidification leading to non-conventional flow effects that explain the time limited peak of AE activity after 500 s. During the current ramp, as the signs

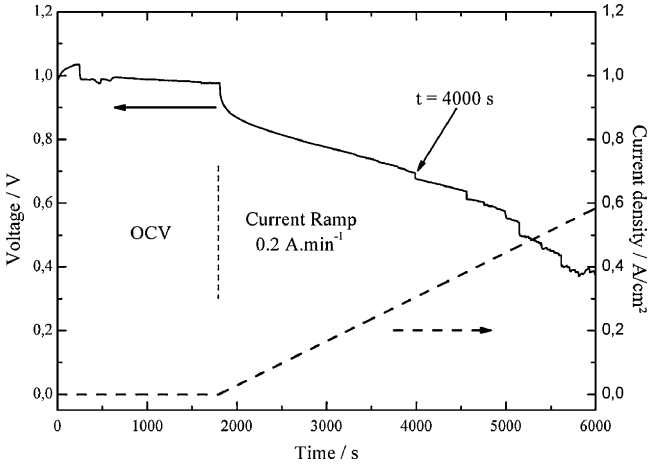

Fig. 13. Time evolution of voltage (black solid line) and current density (blackdashed line) during a current ramp of 0–15 A (O_2 = 0.18 L min^{-1}; H_2 = 0.36 L min^{-1}) gas at 80 °C and fuel cell at 70 °C.

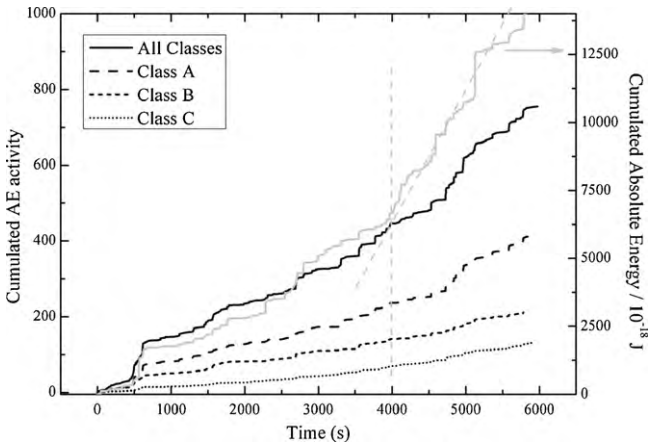

Fig. 14. Cumulated number of AE hits (black, left) and cumulated absolute energy (gray, right) during a current ramp of 0–15 A (O_2 = 0.18 L min^{-1}; H_2 = 0.36 L min^{-1}) gas at 80 °C and fuel cell at 70 °C. Cumulated number of AE events is plotted for each class as described in inset.

of flooding appear on the voltage curve (t > 4000 s), an increase of acoustic emission activity is observed (in terms of cumulated absolute energy or total number of events). This behavior confirms the link existing between AE activity and water transport from MEA to gas channel. At this stage, it is certain that both AL and GDL are saturated with liquid water. The flow of water through the GDL becomes thus proportional to the amount of water produced by the electrochemical reaction. The consequence is the inexorable flooding of gas channels. The application of the supervised pattern recognition method on this AE data set, allows to check the contribution of each class on the global AE activity. The cumulated AE contribution of each class is also plotted in Fig. 14. The results obtained were identified under OCV period as 53.8% coming from class A, 35.1% from class B and 11.1% from class C and during operative condition as 54.9% coming from class A, 25.1% from class B and 21% from class C. The increase in the percentage of class C at the expense of class B is in full agreement with the appearance of phenomena related to water transport within the cell during the current ramp. This experiment provides thus evidences that confirm our classification.

It is worth stressing that results presented here constitute only a first attempt towards the development of a reliable monitoring system of operating PEMFC. It seems however that AE technique, supported by convenient statistical post-treatment, is a powerful technique to identify phenomenological fingertips coming from different physical origins related to the complex and simultaneous ensemble of different phenomena taking place inside the cell assembly. Yet much work is to be done not only towards a deeper comprehension of the phenomena behind AE events and how AE signals reflect changes in the PEMFC operation parameters, but also in which concerns the identification of the simplest classification and pattern recognition algorithm, not forcibly the one held in this preliminary study.

In conclusion, classes A and B are mainly related to liquid water in gas channels and in gas diffusion layer. These phenomena increase when there are more and more liquid water in the fuel cell. The events in class C are difficult to measure and are weak. Indeed, these events are related to phenomena taking place inside the fuel cell and, for the most part, within the membrane. The increase of A, B and especially of C is then a possible indicator of the decrease of fuel cell performances due to flooding.

Nevertheless, AE appears as a very promising tool to the monitoring of operating PEMFC, even if this should obviously require the development of specifically devoted fast software packages.

5. Conclusions

This paper relates a first approach concerning the feasibility of using AE technique as a PEMFC diagnosis and water management tool. Based on previous work that gave evidence of the existence of AE events during Nafion dehydration, different phenomena that can be source of AE activity throughout PEM fuel cell operation were investigated. The aim was to determine in which extent the AE events are characteristic of the source that generates it. In this way, three classes of phenomena were a priori established and studied as individually as possible:

- phenomena related to diphasic phenomena in the gas channel,
- those related to water removal into the GDL,
- and those induced by the water uptake or desorption into the catalyst layer and membrane.

AE has shown good sensitivity to different operating conditions. More particularly, changes in the gas humidification level and the variation of MEA water uptake were closely linked to the evolution of AE activity. Specific experimental procedures allowed the classification of the recorded AE events into these three classes. The examination of the classification performed has shown good agreement between the phenomena that can potentially occur and the repartition of the events into the classes. In other words, it has been shown that AE activity related to distinguishable sources can be recorded online on PEM fuel cell and constitute the starting point of an online and non-invasive PEMFC monitoring strategy, even if much remains to be done to ensure practical application of the technique and to clearly identify specific issues as pinhole formation and fuel starvation. This study may be the subject of future work.

Acknowledgments

This work, including BL doctoral fellowship, has been supported by the *cluster Energie* of *Région Rhône-Alpes*.

References

[1] S.G. Chalk, J.F. Miller, J. Power Sources 86 (2000) 40–51.
[2] S.G. Chalk, J.F. Miller, J. Power Sources 159 (2006) 73–80.
[3] B. Du, Q. Guo, R. Pollard, D. Rodriguez, C. Smith, J. Elter, J. Miner. Met. Mater. Soc. 58 (2006) 45–49.
[4] P. Zegers, J. Power Sources 154 (2006) 497–502.
[5] J. Stumper, C. Stone, J. Power Sources 176 (2008) 468–476.
[6] K. Schoots, G.J. Kramer, B.C.C. van der Zwaan, Energy Policy 38 (2010) 2887–2897.
[7] G. Tian, S. Wasterlain, D. Candusso, F. Harel, D. Hissel, X. François, Int. J. Hydrogen Energy 35 (2010) 2772–2776.
[8] P. König, E. Ivers-Tiffée, J. Power Sources 190 (2009) 121–132.
[9] G. Tian, S. Wasterlain, I. Endichi, D. Candusso, F. Harel, X. François, M.C. Péra, D. Hissel, J.M. Kauffmann, J. Power Sources 182 (2008) 449–461.
[10] M. Hinaje, I. Sadli, J.P. Martin, P. Thounthong, S. Raël, B. Davat, Int. J. Hydrogen Energy 34 (2009) 2718–2723.
[11] J. Wu, X.Z. Yuan, H. Wang, M. Blanco, J.J. Martin, J. Zhang, Int. J. Hydrogen Energy 33 (2008) 1735–1746.
[12] J. Wu, X.Z. Yuan, H. Wang, M. Blanco, J.J. Martin, J. Zhang, Int. J. Hydrogen Energy 33 (2008) 1747–1757.
[13] L. Zhang, M. Pan, S. Quan, J. Power Sources 180 (2008) 322–329.
[14] J. Shi, J. Tian, C. Zhang, Z. Shan, J. Power Sources 164 (2006) 284–286.
[15] U.H. Jung, S.U. Jeong, K.T. Park, H.M. Lee, K. Chun, D.W. Choi, S.H. Kim, Int. J. Hydrogen Energy 32 (2007) 4459–4465.
[16] T. Ous, C. Arcoumanis, Int. J. Hydrogen Energy 34 (2009) 3476–3487.
[17] A. Su, F.B. Weng, C.Y. Hsu, Y.M. Chen, Int. J. Hydrogen Energy 31 (2006) 1031–1039.
[18] X. Li, I. Sabir, J. Park, J. Power Sources 173 (2007) 933–942.
[19] X. Yuan, H. Wang, J.C. Sun, J. Zhang, Int. J. Hydrogen Energy 32 (2007) 4365–4380.
[20] M.A. Rubio, A. Urquia, S. Dormido, J. Power Sources 171 (2007) 670–677.
[21] K. Ito, K. Ashikaga, H. Masuda, T. Oshima, Y. Kakimoto, K. Sasaki, J. Power Sources 175 (2008) 732–738.
[22] F. Barbir, H. Gorgun, X. Wang, J. Power Sources 141 (2005) 96–101.
[23] B.C. Seyfang, P. Boillat, F. Simmen, S. Hartmann, G. Frei, T. Lippert, G.G. Sherer, A. Wokaun, Electrochim. Acta 55 (8) (2010) 2932–2938.

[24] P. Kalyanasundaram, C.K. Mukhopadhyay, S.V. Subba Rao, Practical Acoustic Emission, Alpha Science International Ltd., New Delhi, 2007.
[25] S. Yuyama, in: G.C. Moran, P. Labine (Eds.), Corrosion Monitoring in Industrial Plants Using Nondestructive Testing and Electrochemical Methods, Fundamental Aspects of Acoustic Emission Applications to the Problems Caused by Corrosion, vol. STP908, American Society for Testing and Materials, 1986, p. 43.
[26] M. Boinet, J. Bernard, M. Chatenet, F. Dalard, S. Maximovitch, Electrochim. Acta 55 (2010) 3454–3463.
[27] C. Jirarungsatian, A. Prateepasen, Corros. Sci. 52 (2010) 187–197.
[28] C. Jomdecha, A. Prateepasen, P. Kaewtrakulpong, NDT & E Int. 40 (2007) 584–593.
[29] Y.P. Kim, M. Fregonese, H. Mazille, D. Feron, G. Santarini, Corros. Sci. 48 (2006) 3945–3959.
[30] J. Malzbender, R.W. Steinbrech, J. Power Sources 173 (2007) 60–67.
[31] G. Gebel, Polymer 41 (1999) 5829–5838.
[32] L. Rubatat, A.L. Rollet, G. Gebel, O. Diat, Macromolecules 35 (2002) 4050–4055.
[33] H. Tang, S. Peikang, S.P. Jiang, F. Wang, M. Pan, J. Power Sources 170 (2007) 85–92.
[34] B. Legros, P.X. Thivel, Y. Bultel, M. Boinet, R.P. Nogueira, Electrochem. Solid-State Lett. 12 (2009) B116–B118.
[35] N.N. Hsu, F.R. Breckenridge, Mater. Eval. 39 (1981) 60–68.
[36] I.T. Jolliffe, Principal Component Analysis, 2nd ed., Springer-Verlag, New York, 2002.
[37] S. Theodoridis, K. Koutoumbras, Pattern Recognition, 4th ed., Academic Press, Burlington, 2009.